

EFFECT OF GEOMETRIC CHANGES IN AN IDEALISED CONTACTING BRUSH SEAL BRISTLE PACK ON TYPICAL KEY PERFORMANCE MEASURES

**Michael J Pekris \***

Transmissions, Structures & Drives  
Rolls-Royce plc.  
Derby, DE24 8BJ  
UK

michael.pekris@rolls-royce.com

**Gervas Franceschini**

Transmissions, Structures & Drives  
Rolls-Royce plc.  
Derby, DE24 8BJ  
UK

gervas.franceschini@rolls-royce.com

**David R H Gillespie \***

Department of Engineering Science  
University of Oxford  
Oxford, OX1 3PJ  
UK

david.gillespie@eng.ox.ac.uk

**ABSTRACT**

In an effort to reduce gas turbine specific fuel consumption and to increase specific thrust, advanced sealing technologies have been deployed for the purpose of secondary air flow management. One such technology, the brush seal, provides a more compliant seal and hence improved leakage performance over the legacy industry standard, the labyrinth seal. It is known that brush seal geometry has a strong effect on the loading, deformations, temperatures and flows in the bristle pack. There is limited understanding of the complex interactions between the geometric variables. This paper describes a methodology for the modelling of an idealised brush seal domain based on Computational Fluid Dynamics. Bristle pressure and force distributions, temperature distributions and tip contact forces are presented. This methodology is used to examine the sensitivity of these parameters to the geometric input variables for a contacting seal configuration, using a Design of Experiments approach. Inferences are drawn from the results to determine which of the geometric parameters are most influential in brush seal pack flow-induced behaviour, and the strength of the coupling between these parameters and the key performance indicators.

**NOMENCLATURE**

$d$	bristle diameter, m
$F_z$	net axial force, N
$F_x$	net blow-down force, N
$h_{b,r}$	backing-ring (B.R.) height, m
$L$	bristle length, m
$\dot{m}$	mass flow rate, kg/s
$n$	number of rows
$T$	temperature, K
$x$	coordinate direction perpendicular to bristle local axis
$y$	coordinate direction parallel to bristle local axis
$z$	axial coordinate direction (opposing flow)
$X$	tangential coordinate direction
$Y$	radial coordinate direction
$Z$	axial coordinate direction (opposing flow)
	inter-bristle spacing, m
	bristle lay angle, °
$\phi$	angle around bristle circumference, °

\* Corresponding authors.

## INTRODUCTION

Previous research has demonstrated the superior leakage performance of brush seals over the legacy industry standard, the labyrinth seal [1]. Hence the brush seal [2] has been deployed in gas and steam turbine applications [3, 4] to improve the management of secondary air system flows. This provides significant benefit in terms of specific fuel consumption, operating costs, and CO<sub>2</sub> emissions [5].

Extensive experimental testing and computational modelling of nominal seal designs have been carried out, to gain a fundamental understanding of brush seal physics, with the ultimate aim to achieve reliable and predictable designs that retain their performance over sufficient cycles and hours. Some researchers [6 - 8] model the brush seal bristle pack as a porous medium with calibrated transport coefficients in order to obtain predictions of seal leakage. Numerical studies where the inter-bristle flow is modelled [9 - 11] are more conducive to a detailed analysis of bristle pack flows, bristle aerodynamic loading and conjugate heat transfer. A methodology for obtaining a converged flow and mechanical bending solution, including inter-bristle contact and friction, in order to better represent real bristle pack behaviour has been demonstrated [12]. Consideration has also been given to 3-dimensional bristle bending [13]. Bristle tip temperature at the contact interface is another desirable output from brush seal modelling, and this has been attempted using both analytical models and numerical simulation [14 - 16]. A semi-empirical treatment of brush seal heat transfer has been presented [17].

It is possibly surprising then that in brush seal design, there remains limited understanding of the complex interactions between the brush pack geometric design variables. In this paper, a parametric study is outlined which employs a Design of Experiments approach [18] to achieve efficient coverage of the design space. Computational Fluid Dynamics modelling of the bristle pack, drawing from previous research [9 - 14], forms the basis of the parametric study, and the numerical outputs are processed to obtain key performance measures for comparison between the geometric configurations. Inferences are thus drawn from these data on the significant parameters in brush seal bristle pack design.

## METHODOLOGY

### Geometry and Grid Generation

A family of idealised brush seal domains was created using the commercial meshing package GAMBIT (Version 2.3.16). These comprised a single circumferential bristle row with constant inter-bristle spacing.

The bristles were arranged into a hexagonal close-packed arrangement, as depicted in the cross-section in Fig. 1, which represents the physical arrangement of bristles in a real brush seal prior to pressurization. In a real brush seal, a differential pressure will cause deflection (and tighter packing) of the bristle elements, resulting in a slightly disconfigured bristle arrangement. Even though these deflections change the interstitial gap sizes along the bristle length, and lead to inter-bristle and bristle-backing ring contact, an idealised pack configuration gives a reasonable indication of the expected flow and temperature fields within the pack. Further, forces induced by the

cold build of the seal play a part in changes which take place in the pack geometry as soon as pressurisation commences.

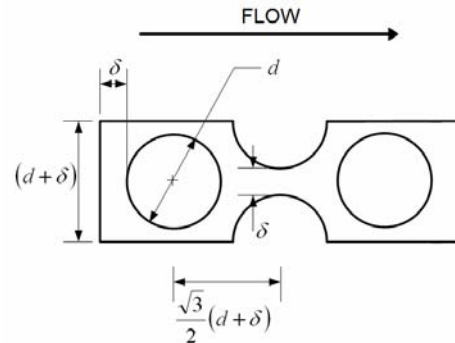


Figure 1. Cross section of bristle pack: hexagonal close packed arrangement of an initial test domain of 3 rows (along bristle axis)

An initial test domain was created that comprised a bristle pack of 3 rows ( $n$ ) and an exit region under a backing ring, shown in Fig. 2. The bristles of diameter ( $d$ ) 142 $\mu$ m, were inclined ( $\theta$ ) at 45° to the radial direction, and spaced 10  $\mu$ m apart ( $\delta$ ) all the way along their length ( $L$ ), which was 2 mm. As such, bristle contact and vanishing fluid volumes were avoided. Bristle spacing was based on pack thickness measurements at the root for a range of test seals and is typical of real bristle packs with high packing efficiency. A length,  $L$ , of 2 mm would be entirely unrealistic in a brush seal, exhibiting high stiffness and no ability to accommodate shaft excursions. However, for the purposes of illustrating the methodology, and under the idealised conditions of rotor-contact with zero bending, a 2 mm bristle length was deemed adequate, this having an additional benefit in minimising the processing time. A gap of  $\delta$  is assumed between the last row of the bristles and the backing ring. The backing ring clearance ( $h_{b,r}$ ) was set at a perpendicular distance of 1 mm from the rotor, or  $\sqrt{2}$  mm away from the tip along the local bristle axis. This reduced backing ring clearance is typical of real brush seals during operation. The flow field in a large scale clearance brush seal has been previously modelled [11]. This study aims at providing further insight into the flow and heat transfer phenomena in contacting brush seals, where frictional heat generation results in high bristle-tip temperatures and a bristle pack temperature distribution.

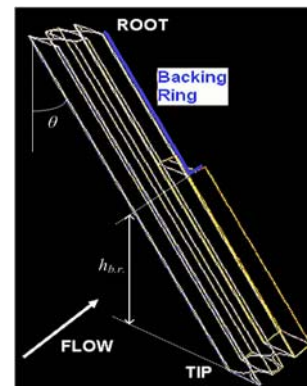


Figure 2. Initial brush seal domain: 3 rows, 2 mm bristles, 45° lay angle, 142  $\mu$ m wire diameter, 10  $\mu$ m bristle spacing, 1 mm backing ring clearance

Domain creation was automated using a parameterised journal file with the six geometric input variables. This approach allowed the careful control of mesh density using both tetrahedral unstructured meshes (within bristle pack) and structured hexahedral meshes (under backing ring), allocated boundary layers, and applied boundary conditions. Higher grid resolution was used in the tip regions and around the last bristle row resulting in a mesh with over 7 million cells. The general approach above used for the initial geometry is illustrated in Fig. 3.

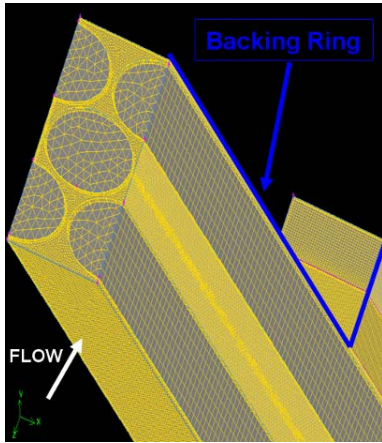


Figure 3. Brush Seal Domain: Hybrid Mesh

A mid-range test pressure of 5 bar total pressure inlet and atmospheric static pressure outlet boundary conditions were defined at the inlet and outlet faces of the domain respectively. Periodic boundaries were attached to the left and right extremities of the

domain effectively creating an infinitely repeating linear brush seal. Heat flux boundary conditions applied at the bristle tips and at the rotor-air interface were calculated from experimental measurements of seal power in brush seals carried out at the University of Oxford, assuming that half of the frictional heat generated was conducted up the solid bristles and convected to the air in-between the bristles. To enable convection of the conducted heat to the air, fluid-solid interfaces were defined on the bristle curved surfaces where the temperatures of the adjacent fluid-solid cells were assumed to be equal in the calculation. This is justified by consideration of the size of the heat transfer coefficient between bristles as set out in [17]. As in the experiment, the fluid temperature at the inlet was set at ambient conditions (300 K). To provide an appropriate heat sink in the initial simulation, and later for the parametric study, the temperatures at the bristle root and backing ring were also set to 300 K. For the purposes of the parametric study, the effect of swirling or tangential flow on the change in the brush seal performance measures is expected to be small as the key geometric inputs are varied. Hence a static wall boundary condition was implemented at the bristle tips for this study.

### Flow Solution

The mesh in Fig. 3 was imported into FLUENT (Version 6.3.26), a commercial code used in the numerical solution of flow and temperature fields. The Navier-Stokes and energy equations were solved using a steady, first order, coupled-implicit finite volume solver. The solution at each iteration was used to update the fluid properties until a converged solution was achieved.

Reynolds number between the bristles, based on bristle diameter, was ~300. This showed that viscous forces generally dominate over inertial forces in the brush seal problem. Hence, a laminar solver was

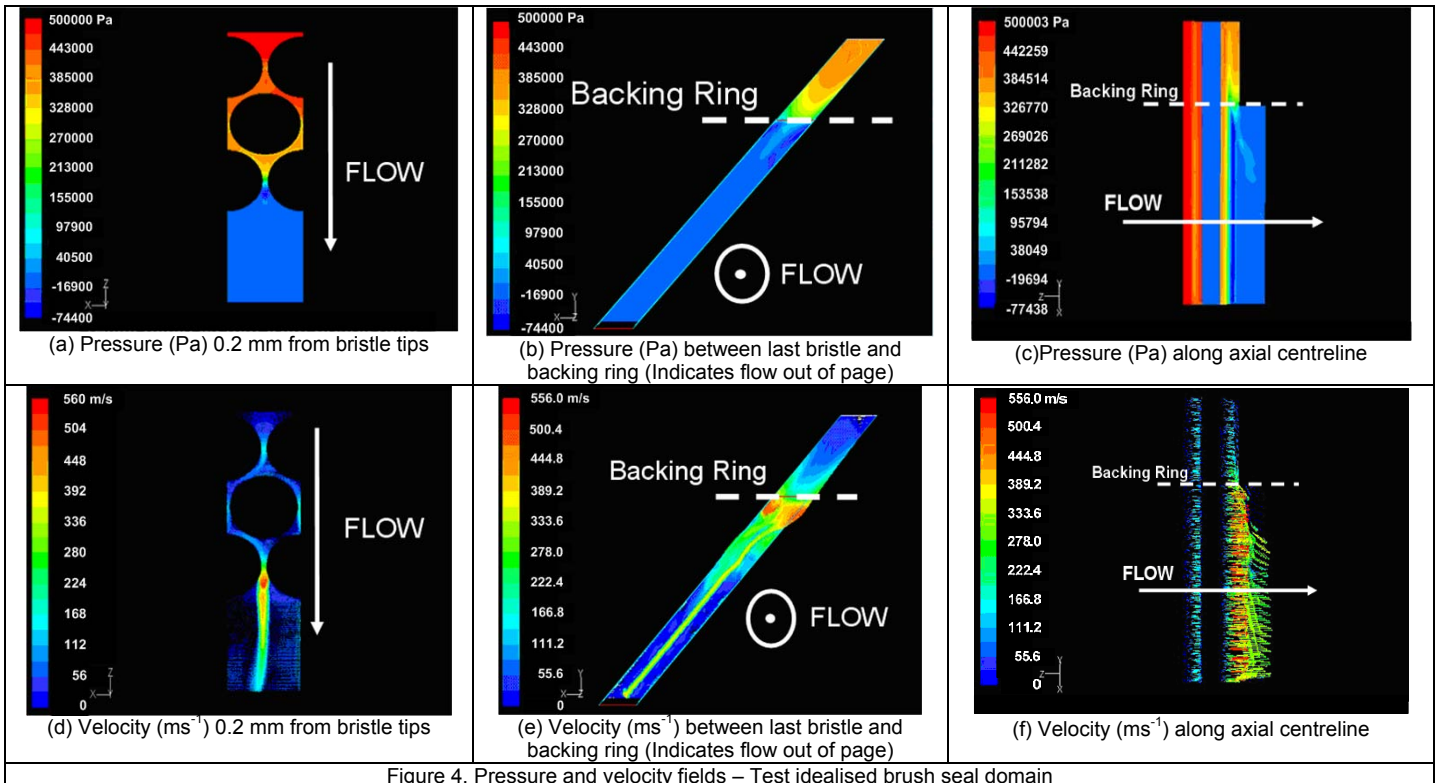


Figure 4. Pressure and velocity fields – Test idealised brush seal domain

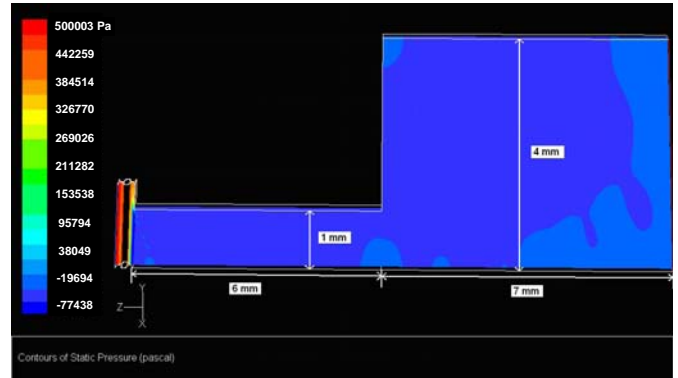
used. Initial simulations produced fluid velocities nearing or at the speed of sound in places, confirming the need for a compressible flow solution. The relevant bristle material properties were used with the solid bristle domains to allow representative heat conduction. Standard properties were used for the working fluid. A converged flow and heat transfer solution was obtained with a convergence criterion of  $1e-4$  on average residuals for mass flux, pressure, velocity and temperature. The size of the mesh was increased from 6 million to 10 million cells, to give an indication of its effect on the flow field and the derived bristle forces and temperature distributions. As variation of less than 10% was obtained, the lower mesh size was considered of sufficient density and resolution. Mesh consistency was ensured (gap- and edge-resolution) to enable direct comparison of the results from the parametric study.

Inspection of the pressure and velocity fields in Fig. 4 shows that the expected brush seal flow features are present in the simulation results. The upper set of figures (Figs. 4a – 4c) show the computed pressure distribution through the fluid domain, and the lower set (Figs. 4d – 4f) give the corresponding velocity vectors.

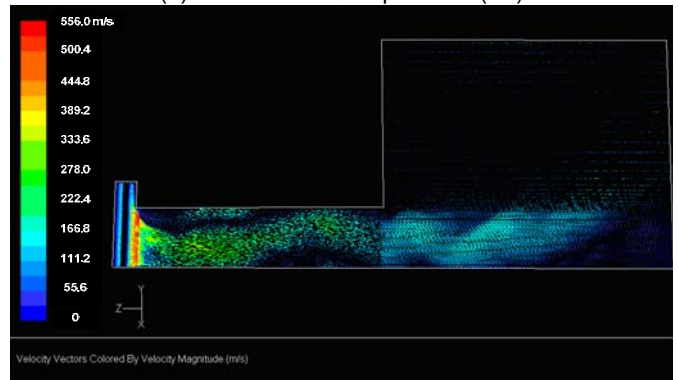
The horizontal slice through the domain (Fig. 4a) shows that the largest pressure drop occurs across the last row of bristles. This is also illustrated in axial slice (Fig. 4c). This, coupled with a rapid expansion in the cross-sectional area, downstream of the bristle pack results in flow jetting immediately and, as indicated in Fig. 4d, velocities in excess of  $500 \text{ m s}^{-1}$ . The vertical slice through the domain (Figs. 4b, 4c and 4e) shows that another region of high pressure gradient is present under the backing ring, causing a rapid acceleration of the flow and high resultant velocities. Hence the gap between the last row of bristles and the backing ring acts as an additional restriction to the flow through the seal, since the critical pressure ratio is also exceeded in the radial direction.

A well known brush seal flow field feature, indicated in the velocity plot in Fig. 4f is that the flow separates from the backing ring at the sharp corner downstream of the bristle pack. An identical simulation was conducted with the domain extended downstream to confirm this. The pressure field is given in Fig. 5a which shows domain dimensions, heights being in the radial direction (at  $45^\circ$  to the local bristle axis). The pressure plot demonstrates the brush seal's pressure holding capability under the idealised conditions of zero axial bending, while the velocity vectors of Fig 5b show that the flow does reattach to the backing ring inner edge further downstream, but exhibits an oscillatory characteristic along the length of the exit passage, due to the original radial component of velocity.

The extension of the domain downstream did not result in significant changes in the bristle pack pressure distribution, and therefore pack forces and temperatures were relatively unaffected. Thus the short downstream passage length was used to define the domain for all further simulations.



(a) Contours of static pressure (Pa)



(b) Velocity vectors ( $\text{m s}^{-1}$ )

Figure 5. Brush Seal Domain: Extended Outlet Region (Above: Pressure, Below: Velocity)

### Bristle Force and Temperature

3-dimensional elemental data extraction from FLUENT was automated using a journal file, and imported into MATLAB for post-processing and analysis. As illustrated in Fig. 6, the local pressure distribution was obtained against bristle length,  $y$ , and angle around the bristle,  $\phi$ . Cylindrical polar coordinates were used to project bristle surface data onto a 2-dimensional grid. The bristle adjacent to the backing ring is analyzed here and in the parametric study, as it experiences the highest pressure gradients and hence forces during operation.  $\phi = 0^\circ$  represents the point on the bristle surface aligned with the incoming flow (negative Z-axis). The result shows that the pressure drops from the root ( $y = 2000 \mu\text{m}$ ) towards the bristle tip ( $y = 0 \mu\text{m}$ ) as expected. On the downstream edge ( $\phi = \pm 180^\circ$ ), bristle pressure drops more suddenly than at the upstream edge ( $\phi = 0^\circ$ ), due to the abrupt pressure drop to atmospheric conditions across the last row of bristles and just below the backing ring ( $y = 1414 \mu\text{m}$ ).

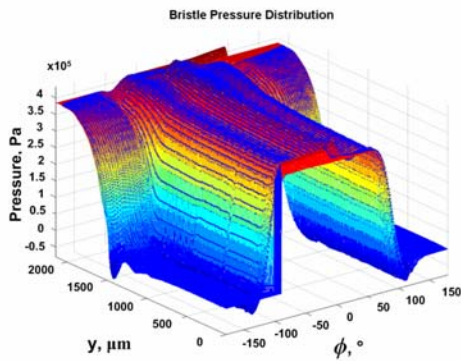


Figure 6. Bristle Pressure Distribution: Last row of bristles (backing ring)

The elemental pressure data were used to derive the axial and radial (blow-down) components of distributed loading, and therefore net force quantities, and it should be noted that pressure differences at the maximum radial location tend towards zero. These are discussed in more detail below.

Resolved shear stress distributions were obtained over the bristle surface. The locations of highest wall shear stress are in the gaps between the bristles ( $\phi = \pm 90^\circ$ ) and just under the backing ring ( $y = 1414 \mu\text{m}$ ,  $\phi = \pm 180^\circ$ ), where there are high flow velocities. Although the contribution of shear forces to total bristle force was less than 5% it was included in the calculation to capture any physical effects in the parametric study.

A similar distribution was obtained for bristle surface temperature, as a function of length and angular position (Fig. 7). The plot shows that the highest temperatures are located at the bristle tip, where the experimentally measured heat flux boundary condition was applied. Circumferential resolution of temperature reveals that the highest tip temperatures are located on the downstream side of the bristle ( $\phi = \pm 180^\circ$ ), in the low pressure region where flow has separated from the bristle surface. The lowest tip temperature is located on the upstream side of the bristle; the flow is brought to rest and a stagnation point results at  $0^\circ$ , allowing very effective heat transfer to occur with the air and hence bristle cooling. The bristle temperature falls rapidly with distance away from the tip and is, thereafter, determined mainly by flow velocity. At  $\phi = \pm 90^\circ$ , a dip in local bristle temperature is seen due to jetting in the gaps between the bristles in the last row.

Local bristle temperature distributions of rows further upstream show a far less pronounced dip in temperature at these angles, due to the lower inter-bristle flow velocities. A significant drop in local bristle temperature is also evident just below the backing ring ( $y = 1474 \mu\text{m}$ ,  $\phi < -90^\circ$ ,  $\phi > -90^\circ$ ), corresponding with the sudden flow acceleration of the flow in this region (Fig. 4).

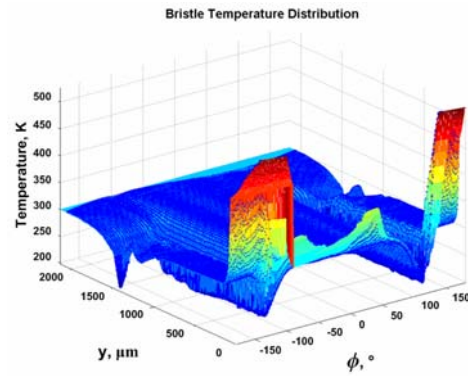


Figure 7. Bristle Temperature Distribution: Last row of bristles (backing ring)

The net pressure and viscous forces were calculated from the numerical integration of the discrete pressure and wall shear stress data. The net axial and blow-down components thus obtained are given in Figs. 8 and 9.

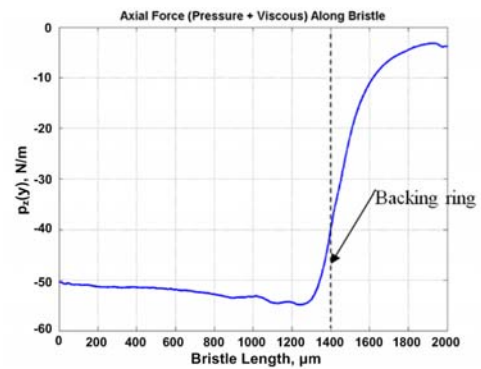


Figure 8. Axial bristle force per unit length: last row of bristles, contacting seal

Fig. 10 shows the circumferentially averaged bristle temperature distribution from the root to the tip. The maximum bristle temperature is observed at the tip ( $y = 0$ ), and this rapidly decreases with distance away from the tip. Just below the backing ring, the highest velocities are observed, and heat transfer causes the local bristle temperature to drop to a minimum just under  $y = 1414 \mu\text{m}$  (the distance of the backing ring from the bristle tip).

Thereafter, the bristle temperature rises steadily to 300 K, where flow velocities are also relatively low. The maximum (bristle tip) temperature, at the tip is further considered in the parametric study.

The variation of the axial and blow-down forces with bristle row is shown in Fig. 11 for the 3-row seal (row 1 is the inlet and 3 is the outlet). The result confirms the hypothesis that the row of bristles adjacent to the backing ring experiences the highest radial and axial loading. Increasing the number of rows would reduce the size of the pressure gradients across the last row of bristles, and hence the magnitude of the resultant forces.

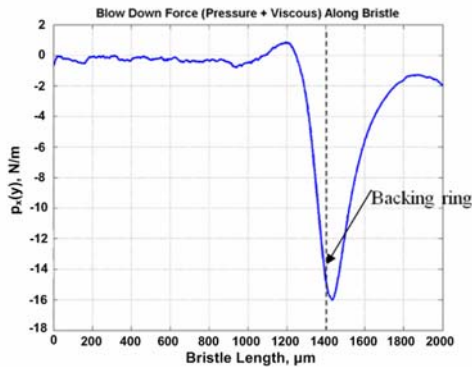


Figure 9. Blow-down bristle force per unit length: last row of bristles, contacting seal

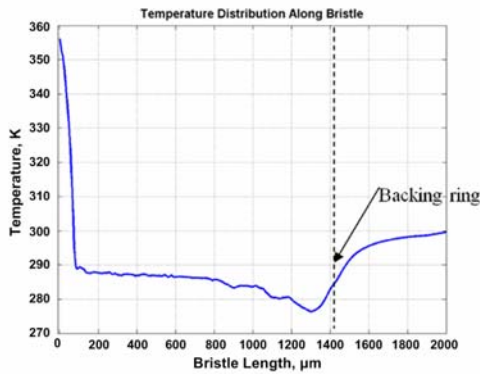


Figure 10. Bristle temperature distribution: last row of bristles, contacting

A root finding algorithm was written and implemented with linear beam bending of a built-in cantilever with a distributed load to calculate the tip reaction force for a zero tip deflection (since bristle tips contact rotor). The iteration converged to  $10^{-15}$  N on tip contact force. Net blow-down force and tip reaction force due to blow-down were examined in the parametric study.

**PARAMETRIC STUDY**

The methodology previously outlined was used as the basis of a parametric study, to determine the effect of brush seal geometry on indicative brush seal performance parameters. This study was intended to determine the sensitivity of the outputs to the geometric inputs, and therefore the emphasis was on their variation rather than their absolute quantities.

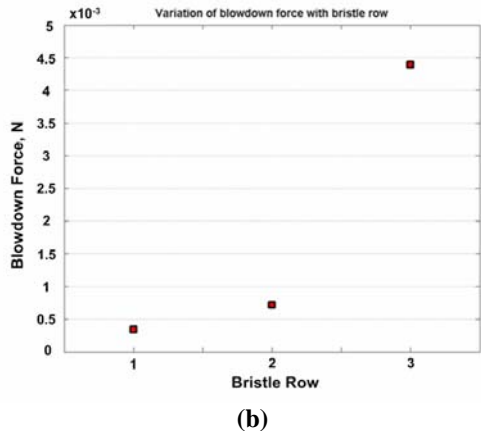
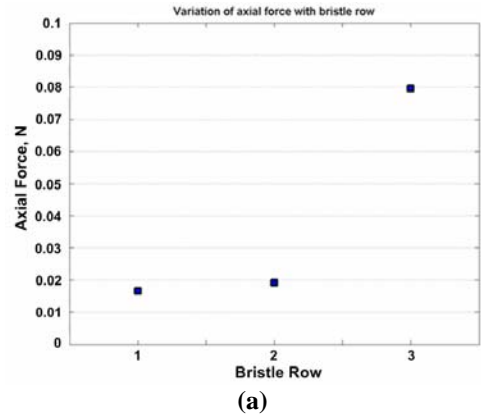


Figure 11. (a) Net axial force vs. Bristle row, (b) Net blow-down force vs. Bristle row

**Design of Experiments**

The six geometric inputs for an idealised brush seal domain are given in Fig. 12, and a proven method of Design of Experiments [18] was used to analyze their effect on the pre-defined outputs. A statistical approach was employed such that the minimum number of CFD simulations was required to ensure full coverage of the design space. A fractional 2-level factorial design was created for the six input variables, and this is given in Table 1. The number of runs was thus reduced from 64 ( $2^6$ ) to 16 combinations of the input variables. A check for non-linearity in the output response was performed by identifying centre points mid-way between the low and high factor levels, and running additional simulations for this geometry. The result for simulation 15 was obtained from the averaged outputs of separate runs with four and five rows of bristles.

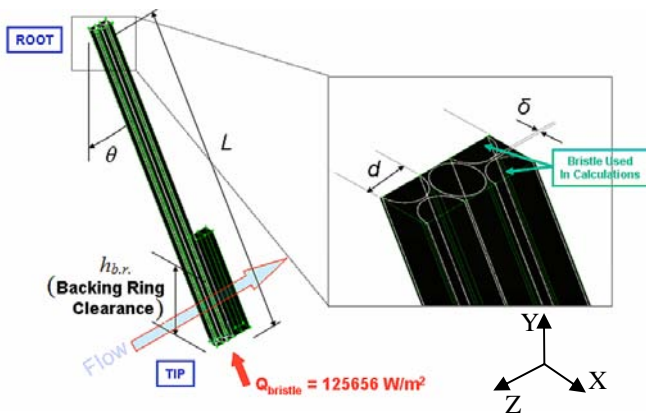


Figure 12. Design of Experiments: Input Variables  
3 axial rows (Z-direction) displayed

The assumed bristle tip heat flux is indicated in Fig. 12. In reality the value of this heat flux would directly relate to tip reaction forces, and thus would partly be dependent on bristle aerodynamic loading. However in this study, this flux was fixed to indicate how bristle pack effectiveness as a heat exchanger varies with geometry, as reflected by the tip temperature. Tip reaction and blow-down forces were also examined to give insight into contact forces and the brush seal's potential for frictional heat generation. Two extended bristle length simulations (18 and 19) were run to ensure that the range for  $L$  was sensible, and that no physical effects were missed. Modelling a representative length of bristle was not expected to change the results significantly, since the largest pressure gradients and the main restrictions to the flow are both in the region of the backing ring, and are the main drivers of flow rate, force and temperature. Sensitivity of the outputs to number of axial rows was obtained for up to  $n = 6$  in order to keep domain size and computation time down.

Table 1. 2-Level Fractional Factorial Design of Experiments with Centre Point

	Length	Spacing	N° of Rows	Lay Angle	Diameter	B.R. Clearance
	$L$	$\delta$	$n$	$\theta$	$d$	$h_{b,z}$
<b>Simulation</b>						
1	3	4	6	30	142	1.2
2	6	4	6	30	71	1.2
3	6	10	6	60	142	1.2
4	6	4	3	30	142	0.8
5	3	4	6	60	142	0.8
6	3	4	3	60	71	1.2
7	6	10	3	30	71	1.2
8	3	10	3	60	142	0.8
9	3	10	3	30	142	1.2
10	6	4	6	60	71	0.8
11	3	10	6	30	71	0.8
12	6	10	6	30	142	0.8
13	6	10	3	60	71	0.8
14	3	10	6	60	71	1.2
15	4.5	8	4.5	45	106.5	1
16	6	4	3	60	142	1.2
17	3	4	3	30	71	0.8
18	7	10	4	60	142	1.2
19	8	8	4	30	71	0.8

Table 2 lists the performance measures used to assess the impact of each of the geometric variables, where  $x$  and  $y$  denote the Cartesian coordinates perpendicular to and aligned with the local bristle axis respectively.  $z$  in the local coordinate system is aligned with  $Z$  in the global coordinate system.

Table 2. Brush Seal Parametric Study Performance Measures

Symbol	Units	Description
$F_z(y)$	N	Net Axial Force
$F_x(y)$	N	Net Blow-down Force
$F_{x,Tip}$	N	Bristle Tip Reaction Force (for zero tip deflection)
$T_{Tip}$	K	Bristle Tip Temperature
$\dot{m}_{exit}$	kg/s	Mass Flow Rate

## RESULTS

### Main Effects

The main effects plots for each of the outputs in Table 2 are presented in Fig. 13 - 18. Main effects plots are a convenient way of assessing the average change of an output with a change of a single geometric input. The outputs generated are averaged at the low and high value of each factor, despite the data being collected with the other geometric inputs changing. Thus these plots should be interpreted with caution, as they do not account for coupled effects of more than one input variable, and hence the reader should also refer to the interaction plots in Figs. 19 - 23. The plots show the raw data (blue) from which the mean data at the low and high values of each parameter (red) are calculated. The centre point (green) provides an indication of non-linearity (henceforth referred to as curvature) in the response of the relevant output variable. The extended length domain cases are also plotted, and these generally fall within the spread of original data indicating that modelling using the short axial domain was appropriate.

Figure 13a shows the main effects of the input variables on net axial force, which is increasing in the negative ( $-z$ ) direction. The mean data, in the plots indicate that net axial force is weakly dependent on bristle length and bristle spacing, but in both cases increases as either length or spacing increase. As mentioned previously, increasing the number of rows reduces the axial force acting on the last bristle row, due to a reduced pressure drop across it. Net axial force is seen to be a stronger function of lay angle, bristle diameter and backing ring clearance. Increasing the lay angle or backing ring clearance increases the free length of bristle that overhangs the backing ring, resulting in a direct increase in net axial force (see Fig. 10). Increasing bristle diameter increases the surface area of the bristle, contributing to a higher net force in the negative  $z$ -direction. These effects appear to be close to linear where the change in force is significant, as the force at the centre point lies close to the linearly interpolated value from the mean data.

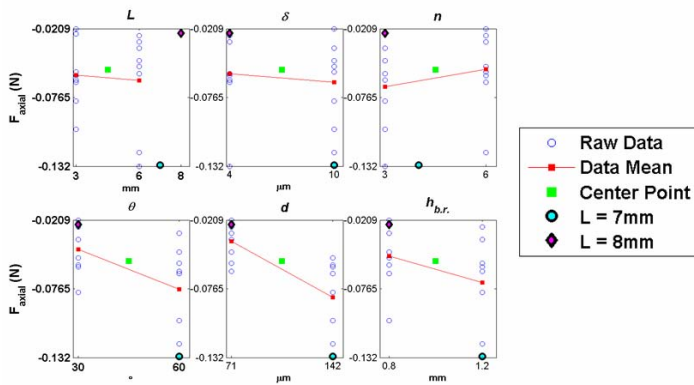


Figure 13. Main Effects: Net Axial Force N

The net blow-down force in Fig. 14 shows a similar response to length, spacing and number of rows. Again, bristle lay angle and bristle diameter induce higher blow-down, as would be expected, but backing ring clearance is shown to have little effect on net blow-down force.

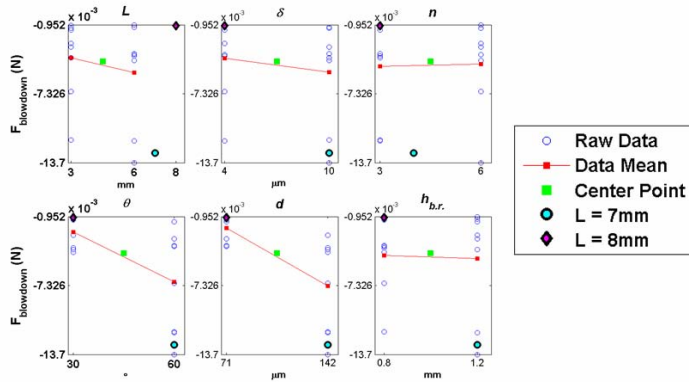


Figure 14. Main Effects: Net Blow-down Force [N]

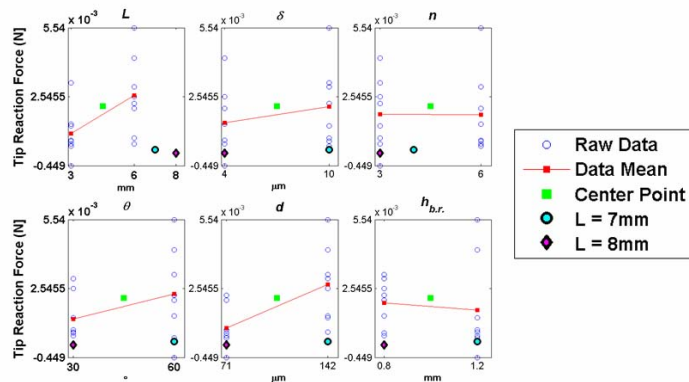


Figure 15. Main Effects: Tip Reaction Force [N]

Figure 15 shows the results of a linear beam bending analysis of a built in cantilever, using the distributed loads outputted from the numerical simulations. Tip reaction force, which is positive in the y-direction, is expected to increase with length due to the larger area

which the distributed load is integrated over. The results of the extended length cases lie within the calculated variance of the core data points. Increasing lay angle and bristle diameter also increases tip reaction force, due to the larger projected area of bristle in the radial direction. This is in agreement with an increasing blow-down force in both cases.

Tip temperature is of significant interest to the designer. As bristle temperatures are mainly influenced by the flow field in and around the bristle pack, Fig. 16 shows a dependence of tip temperature on all six input variables. Of highest significance are bristle spacing and bristle diameter. Higher bristle spacing provides less restriction to the oncoming flow, thus allowing higher velocities and better heat transfer. Significant curvature is suggested by the location of the centre point, indicating either that optimum values exist beyond which there is a reversal in behaviour, or that interactions exist where the effect caused by simultaneously changing another variable dominates that of changing one parameter independently.

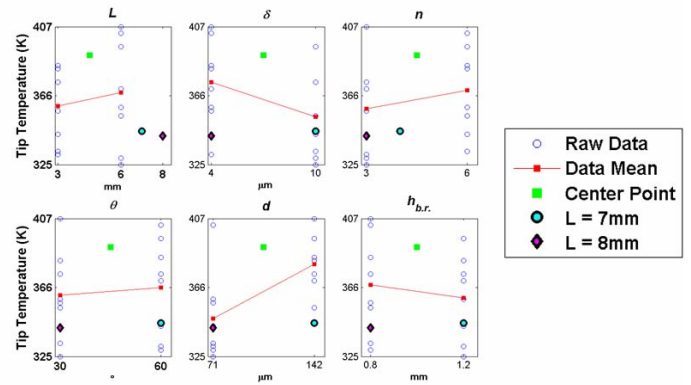


Figure 16. Main Effects Tip Temperature [K]

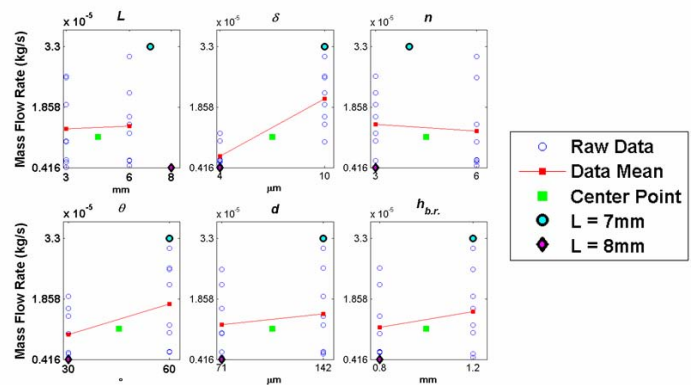


Figure 17. Main Effects: Mass Flow Rate [kg s<sup>-1</sup>]

Figure 17 shows the seal leakage. The mass flow rate sensibly increases with bristle spacing, and the dependency is strong. Increasing the number of rows of bristles generally reduces clearance. Increasing bristle length does not have a profound effect on leakage. Increasing the lay angle and bristle diameter increase the overhang height of the bristle, thus increasing mass flow rate through the

domain. Leakage is also proportional to backing ring clearance, but this is a slightly weaker driver of leakage than the bristle spacing.

### Interactions

The combined effects of the input variables for each output parameter are plotted in Figs. 18 to 22. Interaction plots are used to identify effects in the outputs that are dependent upon more than one geometric input. This is indicated when the effect of a factor on the response changes depending on the value of another factor. The low and high factors, plotted at the data means, are displayed in blue and green according to the legend on the right hand side, and the centre point is plotted in red. Of interest is how the change in a single input on the horizontal axis varies with the value of this factor. Thus, lines of differing gradients (convergent, divergent or crossed lines) indicate an interaction between two variables. The interactions between any two given inputs are indicated by the individual graphs within the plots. Reading across to the right from the first input variable (e.g.  $L$ ) and up from the second (e.g.  $\delta$ ) thus gives the interaction between  $L$  and  $\delta$  with  $\delta$  as the subject. Similarly, reading down from  $L$  and left from  $\delta$  gives the same interaction with  $L$  as the subject.

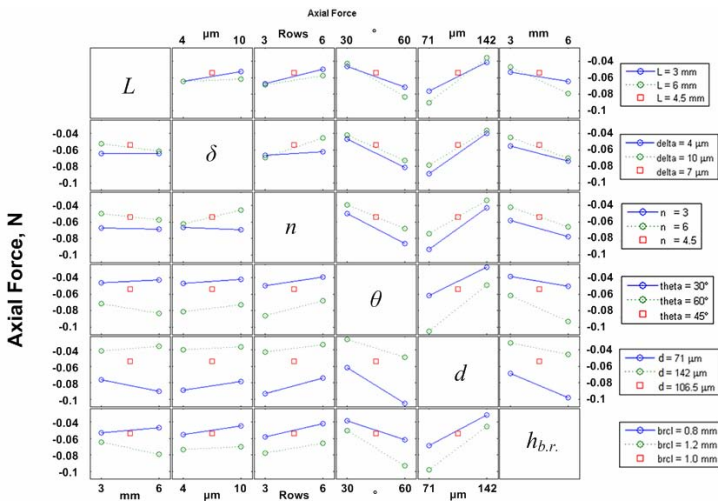


Figure 18. Interactions – Axial Force [N]

Axial force in Fig. 18 generally is driven by weak interactions between variables. Depending on bristle length, the responses to change of the remaining five inputs is only a slight variation in magnitude of the net axial force, though the direction of this change is not uniform. An interaction is observable between number of rows and bristle spacing. At the smaller bristle spacing, which forms a better flow restriction, axial force shows a reduced sensitivity to number of rows, but at the higher bristle spacing, increasing rows reduces the net axial force. Another visible interaction is that between bristle length and lay angle. At the smaller lay angle, an increase in length has little effect on the net axial force, but for a large lay angle the axial force increases.

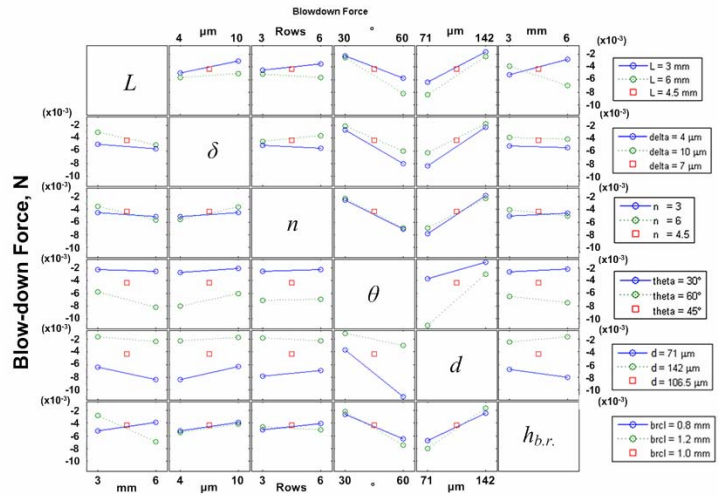


Figure 19. Interactions – Blow-down Force [N]

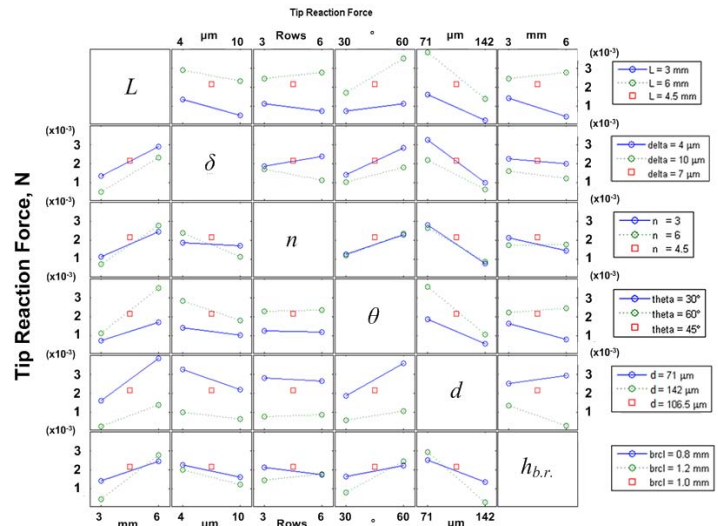


Figure 20. Interactions – Tip Reaction Force [N]

The net blow-down force plots in Fig. 19 show that the strongest interaction is between length and backing ring clearance. At larger backing ring clearances, an increase in length increases blow-down force as would be expected. At lower backing ring clearances, an increase in length reduces the blow-down force, suggesting that if the backing ring height is above a certain percentage of bristle length, behaviour due to the flow field changes. In a real brush seal, this would not normally become a consideration since bristle length would be at least 6 mm. The net blow-down force response to lay angle also varies depending on the value of bristle diameter. Larger bristle diameters make blow-down less sensitive to lay angle. Considering that this effect was derived purely from flow and not mechanical effects, examination of the tip reaction force is also required, Fig. 20. This suggests, as expected, that the stiffer, larger diameter bristle counteracts the effect of an increase in lay angle.

The interaction plots for tip reaction force (Fig. 20) also indicate that larger lay angles make the reaction force more sensitive to  $L$ , as expected. Interactions exist between diameter and backing ring clearance, lay angle and diameter, and length and diameter, indicating that at particular geometric conditions bristle diameter is the dominant determinant of tip force. Another interaction is evident between the number of rows and backing ring clearance, suggesting that the change in backing ring height affects the flow field and therefore bristle loading sufficiently to reverse the sign of the relationship. Additionally, increasing number of rows increases sensitivity to bristle spacing. The plots also suggest that at small lay angles, which would result in a reduced blow-down component of force, backing ring clearance becomes more significant in determining tip reaction force.

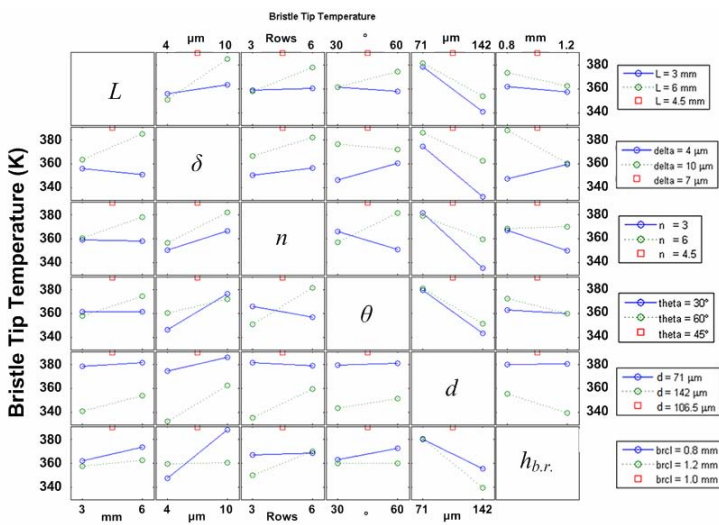


Figure 21. Interactions – Bristle Tip Temperature [K]

Figure 21 shows how the interactions between variables affect bristle tip temperature. The fixed tip heat flux condition represents a single blow-down condition, and thus the trends in these plots are solely a function of the change in flow field. Tip force gives an indication of coupled flow and mechanical phenomena that give rise to heat generation. Tip temperature shows a strong interaction between number of rows and lay angle. Increasing the number of rows is expected to reduce the pressure drop across the last bristle, and hence flow velocities in this region, resulting in an increase in temperature as indicated at  $\theta = 60^\circ$ . At the smaller lay angle, however, CFD shows that increasing the number of rows has the net effect of reducing tip temperature, according to a change in the flow field. This assumes that the variations are linear, but taking into account the position of the centre point, two curves may be produced that overlay reasonably well. Hence further investigation of this interaction is required, with higher order factorial design of experiment or a Cubic Centred Design (CCD). The main effects plots for tip temperature showed a weak overall dependence on bristle lay angle. A notable interaction is present between backing ring clearance and bristle spacing. As expected, at the higher backing ring clearance, which permits a greater

region of higher velocity flow, the bristle spacing becomes less significant in determining heat transfer from the bristle to the air. Backing ring clearance is again shown to be an important parameter in brush seal design through its interaction with number of rows, showing the effect of number rows to be small at a minimum backing ring height of 0.8 mm, which helps to provide the flow restriction. At the length of design interest ( $L = 6$  mm) sensitivity is shown to  $\delta$ ,  $n$  and  $\theta$ . Similarly at the larger bristle diameter, greater sensitivity is shown to  $\delta$  and  $n$ . These and the remaining interactions show similar curvature and should thus be investigated further with a higher resolution design of experiments.

Finally considering leakage mass flow rate (Fig. 22), weak interactions between the geometric variables are generally shown, suggesting that the trends seen in the main effects plots are reasonably accurate. The main exception is an interaction between number of rows and backing ring clearance.

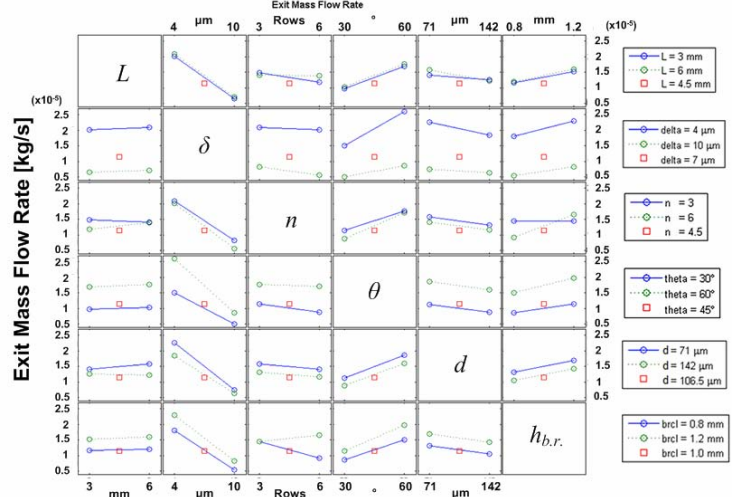


Figure 22. Interactions – Exit Mass Flow Rate [kg/s]

The data for the backing ring clearance of 0.8 mm and the centre point are consistent in showing a reduction in mass flow rate with increasing number of rows, as this is expected to reduce the pressure drop across the last row of bristles. At a backing ring clearance of 1.2 mm, however, seal leakage increases, suggesting a trade-off between the two variables. Another weak interaction is that between bristle spacing and lay angle. The orientation of the bristles has a more significant effect on leakage when the inter-bristle spacing is tighter, suggesting that there is an increase in bristle pressure forces.

## SUMMARY AND CONCLUSIONS

Table 3. Main Effects Summary – Significance Table (Contacting Brush Seal)

[Numbers 1 – 6: order of significance of the effect of each input on a given output variable]

Symbol	$L$	$\delta$	$n$	$\theta$	$d$	$h_{b,r}$
$F_z(y)$	6	5	4	2	1	3
$F_x(y)$	3	4	5	2	1	6
$F_{x,Tip}$	2	4	6	3	1	5
$T_{Tip}$	4	2	3	6	1	5
$\dot{m}_{exit}$	6	1	5	2	4	3

Very Strong Significance  
 Strong Significance  
 Notable Significance  
 Some Significance  
 Insignificant

Tables 3 and 4 summarize the principal main effects and interactions in the CFD study of the idealised brush seal domain. The overall significance of each parameter was calculated based on the gradients of the curves. The main effects table shows that bristle diameter is an important parameter in influencing the flow field in brush seals. The large pressure gradients across the last bristle row increased the sensitivity of net force to bristle diameter in this region. Lay angle also has a strong overall influence on the performance parameters due to its effect on the pack flow and hence bristle aerodynamic loading.

Table 4. Interactions Summary – Significance Table (Contacting Brush Seal)

Output	Interactions						
$F_z(y)$	$L \times h_{b,r}$	$L \times d$	$L \times \theta$	$n \times \delta$	$\theta \times d$	$\theta \times h_{b,r}$	$d \times h_{b,r}$
$F_x(y)$	$L \times h_{b,r}$	$\theta \times d$	$n \times \delta$	$d \times h_{b,r}$	$L \times \theta$		
$F_{x,Tip}$	$d \times h_{b,r}$	$L \times h_{b,r}$	$\theta \times h_{b,r}$	$n \times \delta$	$L \times \theta$	$L \times d$	$n \times h_{b,r}$
$T_{Tip}$	$n \times \theta$	$\delta \times h_{b,r}$	$n \times d$	$L \times \delta$	$L \times n$	$L \times \theta$	$d \times h_{b,r}$
$\dot{m}_{exit}$	$n \times h_{b,r}$	$\theta \times \delta$	$L \times n$				

Very Strong  
 Strong  
 Notable

Tip temperature indicates flow field effects and shows strong sensitivity to bristle diameter and also to bristle spacing, similar to that indicated by leakage. The quantities derived from linear beam bending theory are mainly dependent on bristle dimensions, but there is also a significant influence from bristle spacing and lay angle which affect bristle aerodynamic loading. Tip reaction force indicates frictional heat generation and shows that bristle dimensions are most significant, while sensitivity to bristle spacing (and hence leakage) is also demonstrated. In a real brush seal inter-bristle contact forces, friction and hysteresis would change the bristle pack behaviour. This would alter bristle loading and increase pack stiffness. Tighter packing density (due to compaction under pressure) would restrict leakage through the pack and therefore convective heat transfer, resulting in higher temperatures. The interaction plots showed that the geometric inputs in the idealised brush seal problem can have strong or significant coupled effects on the output. This could change the trends and sensitivities observed in the main effects. Table 4 identifies notable interactions between variables. Coupled effects on the output are shown to be weakest for mass flow rate. Some coupled effects are present for net force, but tip temperature, which is a strong function of the flow field in the bristle pack, exhibits the highest sensitivity to

interactions and trade-offs between variables. The position of the centre point in the tip temperature plots suggested that strong curvature in the responses was possible, and hence further investigation may be required using a higher resolution design of experiments. Tip force and maximum bristle deflection also show high sensitivity to coupled effects, as they are derived from bristle bending which relies on both geometric dimensions and aerodynamic loading. The main effects plots showed backing ring clearance and number of rows to be relatively insignificant, but the interactions show that at the appropriate values of other input variables, these input variables are significant in combination. In general, the designer should be aware that the simultaneous variation of brush seal design variables could result in significant and non-intuitive variation in seal performance. These variations have been identified for the simplest case of an idealised bristle pack in a contacting brush seal.

## ACKNOWLEDGMENTS

The work was funded by Rolls-Royce Plc and the Engineering and Physical Sciences Research Council (EPSRC) and the Technology Strategy Board (TSB), their continued support is greatly appreciated. Help in running and maintaining the CFD clusters at the Osney Thermofluids Laboratory was provided by Rex Belcher.

## REFERENCES

- [1] Steinetz B M, Hendricks R C, Munson S J, “Advanced Seal Technology Role in Meeting Next Generation Turbine Engine Goals”, NASA Report NASA/TM-1998-206961, April 1998
- [2] Ferguson J G, “Brushes as high performance gas turbine seals”. Gas Turbine and Aeroengine Congress, ASME. 88-GT-182, 1988
- [3] Dinc S, Demiroglu M, Turnquist N, Mortzheim J, Gayle G, Maupin J, Hopkins J, Wolfe C, Florin M, “Fundamental Design Issues of Brush Seals for Industrial Applications”, ASME Journal of Turbomachinery, Vol 124, pp. 293 - 300, April 2002
- [4] Neef M, Sulda E, Surken N, Walkenhorst J, “Design Features and Performance Details of Brush Seals for Turbine Applications”, Proceedings of ASME Turbo Expo (GT2006-90404), June 2006
- [5] Chupp R, Hendricks R C, Lattime S B, Steinetz B M, “Sealing in Turbomachinery”, Journal of Propulsion and Power, Vol. 22, No.2, March - April 2006
- [6] Chew J W, Hogg S I, Millener P J, “Porosity Modelling of Brush Seals”, Journal of Tribology, Transactions of the ASME, Vol. 119, pp. 769 - 775, October 1997
- [7] Dogu Y, “Investigation of Brush Seal Flow Characteristics Using Bulk Porous Medium Approach”, Journal of Engineering for Gas Turbines and Power, Transactions of the ASME, Vol. 127, pp 136 - 144, January 2005
- [8] Turner M T, Chew J W, Long C A, “Experimental Investigation and Mathematical Modelling of Clearance Brush Seals”, Journal of Engineering for

- Gas Turbines and Power, Transactions of the ASME, Vol. 120, pp. 573 - 579, July 1998
- [9] Chew J W, Lapworth B L, Millener P J, "Mathematical Modelling of Brush Seals, International Journal of Heat Transfer and Fluid Flow", 16: 493 - 500, 1995
- [10] Chen L H, Wood P E, Jones T V, Chew J W, "Detailed Experimental Studies of Flow in a Large Scale Brush Seal Model and a Comparison with CFD Predictions", Journal of Engineering for Gas Turbines and Power, Transactions of the ASME, Vol. 122 pp. 672 - 679, October 2000
- [11] Franceschini G, Jones T V, Gillespie D R H, "Improved Understanding of Blowdown in Filament Seals", Proceedings of ASME Turbo Expo (GT2008-51197), June 2008
- [12] Lelli D, Cooper P, Chew J W, "Combined 3D Fluid Dynamics and Mechanical Modelling of Brush Seals", Proceedings of ASME Turbo Expo (GT2005-68973), June 2005
- [13] Guardino C, Chew J W, "Numerical Simulation of Three-Dimensional Bristle Bending in Brush Seals", Journal of Engineering for Gas Turbines and Power, Transactions of the ASME, Vol. 127, pp.583 - 591, July 2005
- [14] Chew J W, Guardino C, "Simulation of Flow and Heat Transfer in the Tip Region of a Brush Seal", International Journal of Heat Transfer and Fluid Flow (25 649-658), 2004
- [15] Demiroglu M, Tichy J A, "An Investigation of Heat Generation Characteristics of Brush Seals", Proceedings of ASME Turbo Expo (GT2007-28043), May 2007
- [16] Dogu Y, Aksit M F, "Brush Seal Temperature Distribution Analysis", Proceedings of ASME Turbo Expo (GT2005-69120), June 2005
- [17] Owen A K, Guo S M, Jones T V, "An Experimental and Theoretical Study of Brush Seal and Shaft Thermal Interaction", Proceedings of ASME Turbo Expo, GT2003-38276, June 2003
- [18] Lenth R V, "Quick and Easy Analysis of Unreplicated Factorials", Journal of Technometrics, ASA/ASQ, Volume 31 Issue 4, Nov. 1989
- [19] Long C A, Marras Y, "Contact Forces Under a Brush Seal", Transactions of the ASME (GT-95-211), 1995.